Nanoscale thermal characterization of high aspect ratio gold nanorods for photothermal applications at $\lambda = 1.5$ μ m

Hengyang Xiang, Hung-Ju Lin, Tingting Niu, Zhuoying Chen, Lionel Aigouy

Nanoscale thermal characterization of high aspect ratio gold nanorods for photothermal applications at λ = 1.5 µm

Hengyang Xiang,[1] Hung-Ju Lin,[1] Tingting Niu,[1] Zhuoying Chen,[1,a)] and Lionel Aigouy [1,b)]

[1]*LPEM, ESPCI Paris, PSL Research University, Sorbonne Universités, CNRS, 10 rue Vauquelin, 75005 Paris, France*

We synthetized gold nanorods that present a high aspect ratio (> 10) and possess a surface plasmon resonance in the near-infrared, in the 1300 – 1600 nm spectral range. Using a single Er^{3+}-doped $NaYF_4$ nanocrystal deposited on their surface, we measured the temperature increase of a few nanorods excited at their surface plasmon resonance wavelength. We observed a temperature increase of more than 30 °C for an excitation power density of 3 mW / µm^2. This experiment shows that a very small amount of nanorods can be used for obtaining an intense and localized photothermal effect. Applications can be found in the design of inexpensive infrared photodetectors and photothermal therapy in the third biological window. In addition, the association of gold nanorods to an Er^{3+} doped nanocrystal constitutes a very interesting hybrid heater/temperature sensor.

I. INTRODUCTION

There has recently been an enormous research effort devoted to the chemical synthesis of gold nanostructures and to the study of their optical properties. This interest comes from the presence of localized surface plasmon resonances (LSPR), i.e. collective oscillations of conduction electrons, which give them very special characteristics. When excited at their resonance by incident light, these nanostructures possess an enhanced and localized electromagnetic field, and a strong absorption and scattering peak.[1,2] They found applications in many domains including

a) Electronic mail: zhuoying.chen@espci.fr

b) Electronic mail: lionel.aigouy@espci.fr

catalysis,[3,4] imaging and biosensing,[5-9] solar cells and light emitting devices,[10-12] data storage and magnetic recording,[13] thermo-plasmonics and photothermal therapy.[14-18] In the case of photothermal applications in the field of medicine, the strong absorption that occurs when they are excited at their resonance induces a local heating that can help to treat and cure tumors. For that, it is often suitable to excite between 700 and 900 nm because radiation is weakly absorbed by the tissues in this spectral range.[15,17,18] Other biological windows, located between 1000 and 1370 nm and between 1500 and 1870 nm are also interesting to exploit because the light penetrates better into certain tissues at these wavelengths.[19-22] Note that thermo-optical processes were also studied on thin gold films supporting surface plasmons in the years 2000,[23-26] in various domains such as optoelectronics and microfluidics, thus pioneering the work on nanostructures like nanospheres and nanorods.

Among the different nanostructures that can be used for such photothermal applications, nanorods (NRs) exhibit very interesting properties. Due to their elongated shape, they possess two resonances, one is transverse and is oriented along their short axis (T-LSPR), and the other is longitudinal, oriented along their long axis (L-LSPR). The spectral position of the L-LSPR depends on several parameters like the dielectric environment, and the aspect ratio (AR) which represents the length divided by the width of the rod.[27-30] For Au NRs, the L-LSPR can be tuned from the visible (λ = 650 nm) for an AR of 2 up to the near-infrared (above λ = 1500 nm) for an AR > 10 which make them usable in all biological spectral windows. Up to now, their photothermal properties and their thermal characterization have mainly been studied at an excitation between 650 and 1000 nm.[31-35]

In this article, we present a study of the temperature increase of Au NRs excited at 1.537 µm, which roughly correspond to the third biological window.[21,22] We will show that a few NRs can

produce a local temperature increase of several tens of degrees, making them very efficient heaters in this wavelength range. The temperature elevation is measured using a single fluorescent Er^{3+}-doped $NaYF_4$ nanocrystal (NC) as a nanothermometer deposited at specific locations on the surface with a nanomanipulation system. An interesting aspect of this configuration is that the near-infrared (NIR) laser used for heating the Au NRs is the same than the one that excites the fluorescence of Er^{3+} ions. This very simple mode of operation makes the combination Au NRs / $NaYF_4$:Er^{3+} NC a very powerful and versatile heater / temperature sensor. Note that fluorescent nanocrystals or molecules have already been used recently to determine the temperature of other types of Au nanoparticles, but only in the visible/NIR wavelength range, and on a large amount of nanostructures. This includes $NaGdF_4$:Er/Yb coupled to Au NRs,[35] $(Gd,Yb,Er)_2O_3$ NRs,[36] $NaYF_4$:ErYb NCs[37] coupled to Au nanoparticles, core shell structures $Au/SiO_2/Na(YGd)F_4$:Er/Yb,[38,39] CdSe quantum dots dispersed in solution with various Au nanostructures,[31] and fluorescent molecules.[40,41]

II. Experimental and computational details

A. Synthesis and characterization of Au nanorods

Colloidal Au NRs were synthetized using a modified silver-assisted seed-mediated growth method.[30,42] Details of the synthesis can be found in the supplementary material. We show in Fig. 1(a) the absorption spectrum of gold NRs deposited on a glass (SiO_2) substrate. As shown in the transmission electron microscope (TEM) image in the inset, they have a diameter d = 8.5 ± 1.2 nm and a length D = 94.1 ± 9.8 nm which gives an AR between 10 and 13. The absorption spectrum exhibits a broad peak between 1100 and 1600 nm which corresponds to the L-LSPR of

the rods whereas the smaller peak below λ = 600 nm corresponds to the resonance of unwanted spherical Au particles also formed during the synthesis. The broadness of the L-LSPR peak is likely due to the inhomogeneous size distribution of the NRs, and possibly to NRs aggregation as they were deposited on a substrate. All these effects tend to enlarge the global resonance on a 500 nm wide spectral window. The position of the L-LSPR peak is also in good agreement with other measurements recently performed on NRs with similar large AR.[29]

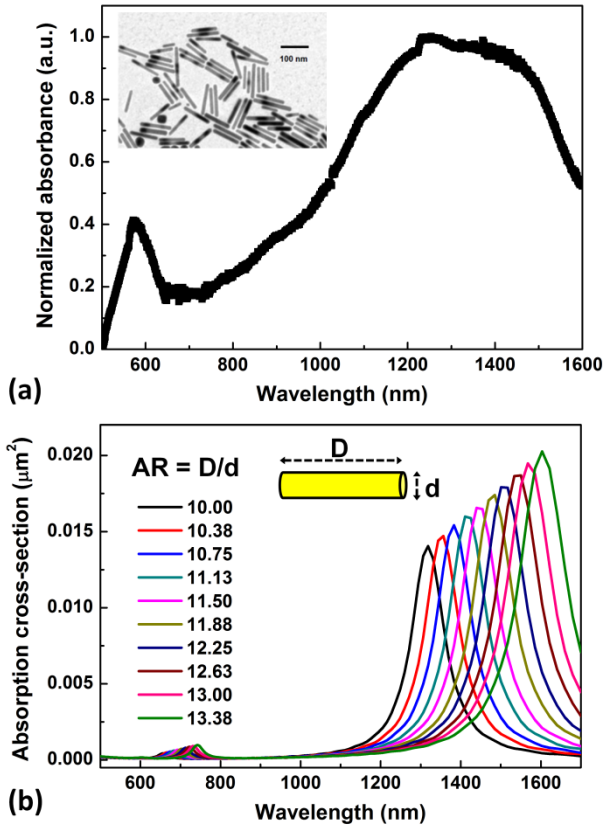

Figure 1: (a) Normalized absorbance of Au NRs spin-coated on a SiO_2 substrate. Inset: TEM picture of the NRs. They have an AR of ~10-13, and a L-LSPR peak between 1100 and 1600 nm; (b) FDTD calculation of the absorption cross-section of isolated Au NRs on a SiO_2 substrate

as a function of their AR. Their diameter was fixed to 8 nm, and their length is varied between 80 and 110 nm.

B. Numerical simulation details

To check the spectral position of the L-LSPR, we calculated by finite difference time domain (FDTD) the absorbance of Au NRs of different AR deposited on a SiO_2 substrate. The simulations were performed using Lumerical commercial software.[43] For the calculation, the Au NRs are placed on a SiO_2 substrate and are supposed to be isolated from each other. We consider that the incident source is a polychromatic plane wave, from 500 nm to 1700 nm, and polarized along the long axis of the Au NR. For the simulation region, the space-mesh size we applied is 1 nm in order to balance our calculation time and geometry description of these nanostructures. As shown in Fig. 1(b) the peak position is found to be in the same wavelength range than in the experiments, i.e. between 1300 and 1700 nm for an AR between 10 and 13. Note that if NRs are separated by only a few nanometers or even if they are in mechanical contact with each other, near-field coupling effects may appear and could shift the resonance furthermore toward the NIR.[44] This means that NRs of smaller AR could have their resonance in the same wavelength range, and thus also contribute to the wide experimental absorbance spectrum of Fig. 1(a).

C. Synthesis of Er^{3+} doped $NaYF_4$ fluorescent nanocrystals

$NaYF_4$ NCs doped with Er^{3+} ions were synthesized by modifying the typical hydrothermal method described in ref 45. The relative composition was 85% of Y and 15% of Er. The nanocrystal had an hexagonal phase and their diameter was around 230 nm. Details of the synthesis can be found in the supplementary material.

D. Thermal and fluorescence experimental setup

The experimental set-up for measuring the luminescence of Er^{3+}-doped $NaYF_4$ NC is shown in Fig. 2(a). Excitation was performed with a continuous-wave infrared laser diode (λ = 1537 nm) focused on the surface in a transmission mode on a 2 µm wide spot. After absorption by up-conversion, the laser radiation is emitted by luminescence in the visible range. The sample was set on a piezo-electric scanning stage (PI) for scanning. The fluorescence was collected by a large numerical aperture (NA) objective (Olympus, x100, NA = 0.8) and sent to a spectrometer (Jobin-Yvon, Triax) connected to a nitrogen-cooled CCD camera (Jobin-Yvon, Symphony). During a scan, a luminescence spectrum was measured at every position of the laser on the surface. The acquisition time was set to ~1 s per point. And the sample scanning and spectrum measurements were synchronized and driven with a homemade Labview program.

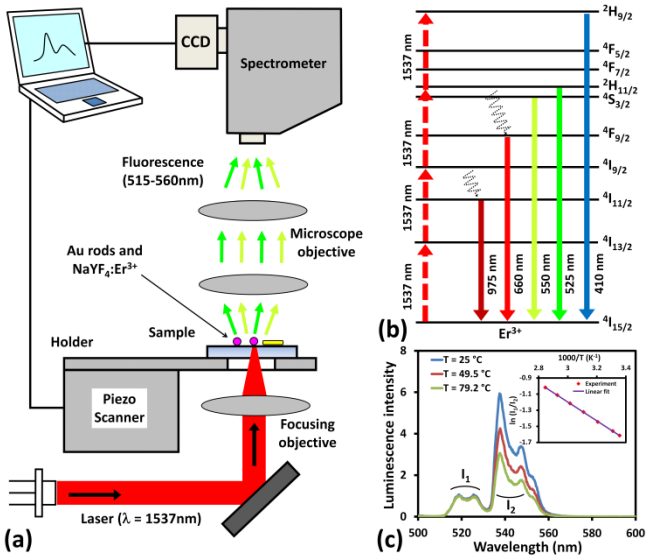

Figure 2: a) Experimental set-up for fluorescence measurements, b) energy band diagram and simplified energy transfers in Er^{3+} ions excited at 1537 nm, c) luminescence spectra of $NaYF_4$: Er^{3+} NC at 25°C, 49.5°C and 79.2°C. The inset shows the evolution of $\ln(I_1/I_2)$ as a function of the inverse temperature.

E. Temperature dependence of luminescence and calibration

The band diagram describing the energy transfers[46] and a room temperature (RT, $T_{RT} \cong 298$ K) luminescence spectrum of the $NaYF_4$:Er^{3+} NCs excited at $\lambda = 1537$ nm are shown in Fig. 2(b) and 2(c) respectively. In our case, we are interested in two particular emission lines, located between 510 nm and 532 nm (green), and between 532 nm and 560 nm (yellowish-green). The green line, further referred as I_1, comes from the transition from the excited $^2H_{11/2}$ state to the $^4I_{15/2}$ state. The yellowish-green line, ~5 times more intense at room temperature than the green one, and further referred as I_2, comes from the de-excitation from level $^4S_{3/2}$ to the ground state. The infrared excitation is non-linear and involves the absorption of several photons. However, the emitted luminescence intensity does not exactly scale as P^n where n is the number of photons ($n = 3$ in the case of green emission) but rather as $\sim P^1$. This behavior has been studied recently and is explained by the relative difference between the decay rates of the intermediate and final energy levels during the up-conversion process.[47,48] It also depends on the power used for the excitation. Here, we are mostly concerned with the temperature dependence of the NC luminescence. Peaks I_1 and I_2 are linked to two transitions whose excited energy levels are in thermal equilibrium.[49-54] When the temperature increases, $^4S_{3/2}$ depopulates in favor of $^2H_{11/2}$, and this causes a relative decrease of I_2 with regard to I_1. The ratio I_1/I_2 is linked to temperature by the following relation:[49-54]

$$\frac{I_1}{I_2} = Ae^{-B/T} \quad (1)$$

where A and B are constants, T is the temperature in K, and I_1 and I_2 are the intensities integrated in the ranges [510-532] and [532-565]. From the intensity ratio of these peaks, and after a proper calibration, it is possible to retrieve the absolute temperature of the NCs. The evolution of the luminescence as a function of T is shown in Fig. 2(c). For this calibration, the NCs were spin-coated on a Si substrate placed on a Peltier stage whose temperature was regulated and measured using a Pt100 thermoresistor. In that case, the laser excitation was achieved in the reflection mode at oblique incidence (not represented here). The evolution of $\ln(I_1/I_2)$ as a function of $1000/T$ is given in the inset of Fig. 2(c). We fitted the experimental data with eq. (1) and determined the value of parameters A and B. A is a constant that depends on the environment near the NC and also on the excitation power. It requires to be slightly adjusted every time the sample or the power is changed. More information about the influence of the excitation power is given in the supporting information. B is the important parameter which rules the temperature dependence of luminescence. It is linked to the energy separation between the two peaks. From the fit shown in the inset of Fig. 2(c), we found A ≅ 10.1 and B = 1170 ± 100 K, in agreement with previous studies with similar Er^{3+}-doped NCs.[54,55]

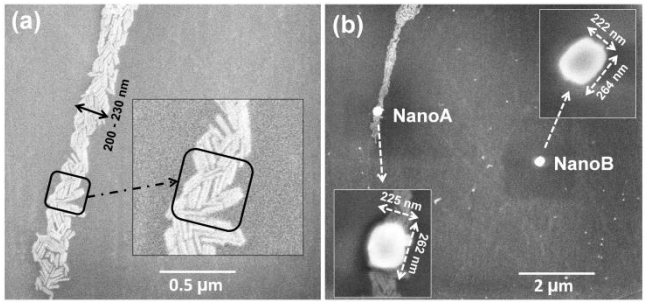

Figure 3: a) SEM picture of Au NRs deposited on SiO_2 substrate, b) SEM picture of the same zone after the deposition of two luminescent $NaYF_4$: Er^{3+} NCs on the surface. NanoA is on the NRs and NanoB is 5 µm away from them.

F. Sample fabrication

In order to study the photothermal properties of Au NRs and their heating capabilities at this excitation wavelength, we fabricated a sample made of only some tens of NRS concentrated in a small region on the SiO_2 substrate. To measure their temperature elevation following an external laser illumination, we used a single $NaYF_4$:Er^{3+} NC as a sensor deposited on their surface. A scanning electron microscope (SEM) image of the rods prior to the NC deposition is shown in Fig. 3(a). The NRs are grouped in a 200 nm wide line. They are not oriented in the same direction although some of them are parallel and in contact with each other's. In Fig. 3(b), we show the same NRs after the deposition of two NCs, deposited with a nanomanipulation system.[56] One NC (furthered referred as NanoA) was directly placed on the NRs and the other (further referred as NanoB) was positioned ~5 µm away on the SiO_2 surface. The role of NanoB is to act as a reference thermometer, insensitive to plasmonic heating.

III. Results and discussion

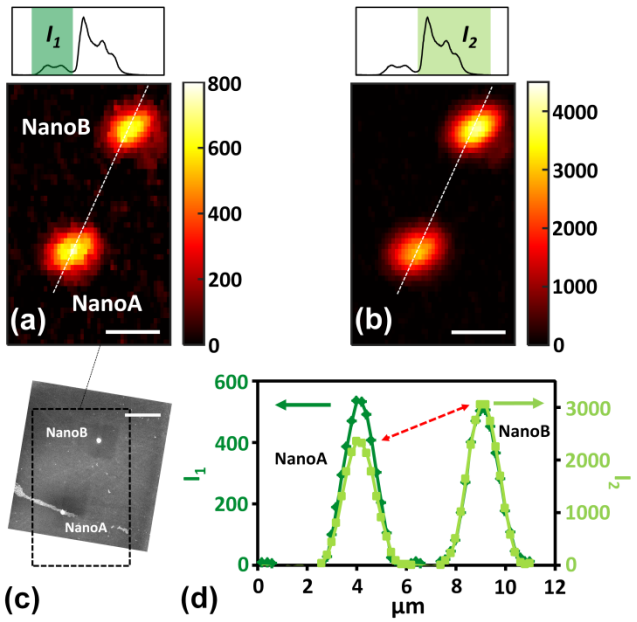

Figure 4: a) Luminescence map around NanoA and NanoB in the I_1 spectral region, b) luminescence map of the same zone in the I_2 spectral region, c) SEM picture of the scanned zone, d) cross-sections extracted from a) and b). The excitation power density was 2 mW / µm^2. The scale bar is 2 µm.

The surface was excited with the configuration shown in Fig. 2. By moving the sample, we first scanned an area of 6 × 10 µm^2 that includes NanoA and NanoB. We show in Fig. 4(a) and 4(b) the measured luminescence maps for an excitation power density of ~2 mW / µm^2. The maps exhibit two bright spots corresponding to NanoA and NanoB [see the SEM picture in Fig. 4(c)]. Their size is limited by the diameter of the incident laser spot on the surface. Cross-sections extracted from the images are shown in Fig. 4(d). Luminescence was separated and integrated into two spectral zones, corresponding to I_1 and I_2. The intensity of I_1 is around 5 times smaller than I_2. From these images, we can see that Nano A and Nano B have roughly the same intensity

in the I_1 spectral range. On the other hand, the intensity of NanoA in the I_2 spectral range is reduced compared to NanoB [see the red arrow in Fig. 4(d)]. This different behavior is an evidence of the heating induced by NRs located under NanoA. After absorption of light, the NRs transfer their heat to NanoA and this induces a relative decrease of I_2 compared to I_1. By dividing the image of Fig. 4(a) by the one of Fig. 4(b), we can map the ratio I_1/I_2 and convert it to a temperature scale using (1). The resulting temperature map and cross-sections are shown in Fig. 5(a) and 5(b). For clarity, the zones in which there were no luminescence (outside NanoA and NanoB) were eliminated. The temperature of NanoA is found to be around 322 K whereas it remains near room temperature for NanoB. We also measured the temperature elevation of NanoA as a function of the laser power density without moving the sample [see Fig. 5(c)]. More details regarding the temperature determination are given in the supplementary information. For a power density close to 3 mW / µm^2, we observed that T increases up to 332 K, i.e. ΔT = 34 K with respect to RT.

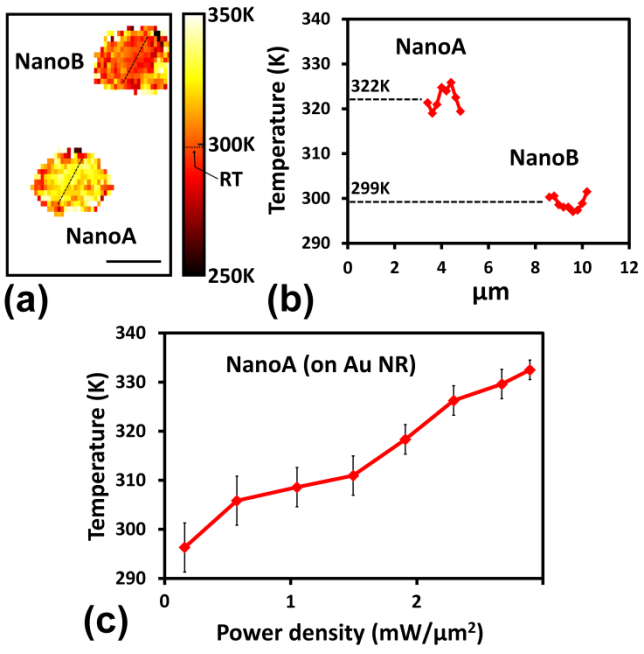

Figure 5: a) temperature map around NanoA and NanoB for an excitation power density of 2 mW / μm^2, b) cross-section extracted from a) showing the temperature increase of NanoA, c) evolution of the temperature of NanoA as a function of the power density. The scale bar in (a) is 2 µm. Room Temperature is around 298 K.

It would be interesting to determine the temperature from numerical simulations and to compare it to the measured value. However, this seems to be very difficult due to the complexity of the experimental configuration. Modeling would be possible with a simple analytical model such as the one described in ref. 14 if a single NR was illuminated. But in our case we have to deal with several NRs very close to each other and all of them contribute to the heating collectively. A more sophisticated model described in ref. 57 allows to handle several plasmonic nanostructures deposited on a surface, but they have to be separated by a certain distance to avoid strong coupling. In our case, such model is not valid because the NRs are separated by only a few nanometers (see Fig. 3) and near-field coupling effects which can change the absorption cross section may occur. Finally, there is a possible temperature difference between the NRs and the NC because the heat transfer channels are not fully efficient. One of them is achieved by direct contact between the two bodies and the other one occurs through the air gap in the interstices between the NRs and the NC or laterally by the sides. The relative importance of such channels depends on the size of the interstices, and on the roughness of the interfaces. The presence of a thermal resistance between the two bodies can also alter the efficiency of the heat transfer by direct contact. These issues are well known in nanothermics and in scanning thermal microscopy where the measured temperature is the one of the probe, not that of the sample.[58] For determining

the real temperature of the NRs, more complex simulations, made by a finite element method, are necessary, but are not the scope of this article.

IV. Conclusions

We investigated the photothermal properties of high aspect ratio Au NRs (AR >10). They possess a L-SPR in the near-infrared region near 1.5 µm, and can be easily excited with a low-cost IR laser diode. We measured the temperature elevation of a few NRs by depositing a single Er^{3+} doped $NaYF_4$ nanoparticle on their surface. At a power of 3 mW / μm^2, we measured a temperature elevation of 34 K which shows the good capabilities of such nanostructures for achieving a local heating at this excitation wavelength. Applications can be found in the domain of photothermal therapy in the third biological window, or for designing inexpensive near-infrared detectors that use photothermal effect. The association nanorod/nanocrystal constitutes also a very efficient heater/temperature sensor. In order to gain in sensitivity and temperature accuracy, it would be interesting to use smaller luminescent nanocrystals directly chemically attached to nanorods for ensuring a good thermal transfer.

Supplementary material

See supplementary material for details regarding NRs and NCs synthesis, for temperature calibration procedures, and for a comparison with other measurements on similar structures.

Acknowledgments

SEM characterizations performed were supported by the region Île-de-France in the framework of DIM Nano-K. H.X. acknowledges the China scholarship council (CSC) for Ph.D. thesis scholarship.

References

[1]M. Pelton, J. Aizpurua and G. Bryant, Laser & Photon. Rev. 2, 136 (2008).

[2]K. M. Mayer and J. H. Hafner, Chem. Rev. 111, 3828 (2011).

[3]J. R. Adleman, D. A. Boyd, D. G. Goodwin and D. Psaltis, Nano Lett. 9, 4417 (2009)

[4]Nianqiang Wu, Nanoscale 10, 2679 (2018).

[5]S. T. Sivapalan, B. M. DeVetter, T. K. Yang, T. van Dijk, M. V. Schulmerich, P. Scott Carney, R. Bhargava and C. J. Murphy, ACS Nano 7, 2099 (2013).

[6]I. H. El-Sayed, X. Huang and M. A. El-Sayed, Nano Lett. 5, 829 (2005).

[7]K. Saha, S. S. Agasti, C. Kim, X. Li and V. M. Rotello, Chem. Rev. 112, 2739 (2012).

[8]Y. Hu, L. Zhang, Y. Zhang, B. Wang, Y. Wang, Q. Fan, W. Huang and L. Wang, ACS Appl. Mater. Interfaces 7, 2459 (2015).

[9]E.S. Shibu, N. Varkentina, L. Cognet and B. Lounis, Adv. Sci. 4, 1600280, 1 (2017).

[10]H. A. Atwater and A. Polman, Nat. Materials 9, 205 (2010).

[11]J. Peng, X. Xu, Y. Tian, J. Wang, F. Tang and L. Li, Appl. Phys. Lett. 105, 173301 (2014).

[12]K. Ueno, T. Oshikiri, Q. Sun, X. Shi and H. Misawa, Chem. Rev. 118, 2955 (2018).

[13]B. C. Stipe, T. C. Strand, C. C. Poon, H. Balamane, T. D. Boone, J. A. Katine, Jui-Lung Li, V. Rawat, H. Nemoto, A. Hirotsune, O. Hellwig, R. Ruiz, E. Dobisz, D. S. Kercher, N. Robertson, T. R. Albrecht and B. D. Terris, Nat. Phot. 4, 484 (2010).

[14]G. Baffou, R. Quidant and F. J. Garcia de Abajo, ACS Nano 4, 709 (2010).

[15]G. Baffou and R. Quidant, Laser & Photonics Reviews 7, 171 (2013).

[16]N. S. Abadeer and C. J. Murphy, J. Phys. Chem. C 120, 4691 (2016).

[17]X. Huang, I. H. El-Sayed, Wei Qian and M. A. El-Sayed, J. Am. Chem. Soc. 128, 2115 (2006).

[18]E. B. Dickerson, E. C. Dreaden, Xiaohua Huang, I. H. El-Sayed, Hunghao Chu, S. Pushpanketh, J. F. McDonald and M. A. El-Sayed, Cancer Lett. 269, 57 (2008).

[19]A. M. Smith, M. C. Mancini and S. Nie, Nat. Nanotech. 4, 710 (2009).

[20]E. Hemmer, N. Venkatachalam, H. Hyodo, A. Hattori, Y. Ebina, H. Kishimoto and K. Sogaab, Nanoscale 5, 11339 (2013).

[21]A. Skripka, A. Benayas, R. Marin, P. Canton, E. Hemmer and F. Vetrone, Nanoscale 9, 3079 (2017).

[22]E. Hemmer, A. Benayas, F. Légaré and F. Vetrone, Nanoscale Horiz. 1, 168 (2016).

[23]A. L. Lereu, A. Passian, J-P. Goudonnet, T. Thundat and T. L. Ferrell, Appl. Phys. Lett. 86, 154101 (2005).

[24]A. Passian, A. L. Lereu, R. H. Ritchie, F. Meriaudeau, T. Thundat, and T. L. Ferrell, Thin Solid Films 497, 315 (2006).

[25]R. H. Farahi, A. Passian, T. L. Ferrell, and T. Thundat, Optics Letters 30 (6), 616 (2005).

[26]A. Passian, S. Zahrai, A. L. Lereu, R. H. Farahi, T. L. Ferrell, and T. Thundat, Phys. Rev. E 73, 066311 (2006).

[27]M. Hu, J. Chen, Z. Y. Li, L. Au, G. V. Hartland, X. Li, M. Marquez and Y. Xia, Chem. Soc. Rev. 35, 1084 (2006).

[28]X. Ye, L. Jin, H. Caglayan, J. Chen, G. Xing, C. Zheng, V. Doan-Nguyen, Y. Kang, N. Engheta, C. R. Kagan and C. B. Murray, ACS Nano 6, 2804 (2012).

[29]H.-H. Chang and C. J. Murphy, Chem. Mater. 30, 1427 (2018).

[30]H. Xiang, T. Niu, M. Schoenauer-Sebag, Z. Hu, X. Xu, L. Billot, L. Aigouy and Z. Chen, Small 14, 1704013 (2018).

[31]L. M. Maestro, P. Haro-Gonzalez, A. Sanchez-Iglesias, L. M. Liz-Marzan, J. Garcia Solé and D. Jaque, Langmuir 30, 1650-1658 (2014).

[32]M. A. Mackay, M. R. K. Ali, L. A. Austin, R. D. Near and M. A. El-Sayed, J. Phys. Chem. B 118, 1319 (2014).

[33]Z. Qin, Y. Wang, J. Randrianalisoa, V. Raeesi, W. C. W. Chan, W. Lipinski, and J. C. Bischof, Scientific Reports 6, 29836 (2016).

[34]W. Albrecht, T.-S. Deng, B. Goris, M. A. van Huis, S. Bals, and A. van Blaaderen, Nano lett. 16, 1818 (2016).

[35]S. Rohani, M. Quintanilla, S. Tuccio, F. De Angelis, E. Cantelar, A. O. Govorov, L. Razzari, and F. Vetrone, Adv. Opt. Mater. 3, 1606 (2015).

[36]M. L. Debasu, D. Ananias, I. Pastoriza-Santos, L. M. Liz-Marzán, J. Rocha and L. D. Carlos, Adv. Mater. 25, 4868 (2013).

[37]A. R. Miandashti, M. E. Kordesch and H. H. Richardson, ACS Photonics 4, 1864 (2017).

[38]Y. Huang, F. Rosei, and F. Vetrone, Nanoscale 7, 5178 (2015).

[39]K. Nigoghossian, S. Ouellet, J. Plain, Y. Messaddeq, D. Boudreau, and S. J. L. Ribeiro, J. Mater. Chem. B 5, 7109 (2017).

[40]G. Baffou, M. P. Kreuzer, F. Kulzer, and R. Quidant, Opt. Exp. 17, 3291 (2009).

[41]S. Maity, W.-C. wu, C. Xu, J. B. Tracy, K. Gundogdu, J. R. Bochinski, and L. I. Clarke, Nanoscale 6, 15236 (2014).

[42]X. Ye, C. Zheng, J. Chen, Y. Gao, C. B. Murray, Nano Lett. 13, 765 (2013).

[43]Lumerical Inc., Vancouver, BC V6E 2M6, Canada, https://www.lumerical.com (accessed January 2019).

[44]A. M. Funston, C. Novo, T. J. Davis and P. Mulvaney, Nano Lett. 9, 1651 (2009).

[45]J. Zhao, Y. Sun, X. Kong, L. Tian, Y. Wang, L. Tu, J. Zhao and H. Zhang, J. Phys. Chem. B 112, 15666 (2008).

[46]S. Ivanova and F. Pellé, J. Opt. Soc. Am. B 26, 1930 (2009).

[47]J. F. Suyver, A. Aebischer, S. García-Revilla, P. Gerner and H. U. Güdel, Phys. Rev. B 71, 125123 (2005).

[48]G. Chen, T. Y. Ohulchanskyy, A. Kachynski, H. Ågren and P. N. Prasad, ACS Nano 5, 4981 (2011).

[49]C. D. S. Brites, P. P. Lima, N. J. O. Silva, A. Millan, V. S. Amaral, F. Palacio and L. D. Carlos, Nanoscale 4, 4799 (2012).

[50]Y. Huang, A. Skripka, L. Labrador-Páez, F. Sanz-Rodríguez, P. Haro-González, D. Jaque, F. Rosei and F. Vetrone, Nanoscale 10, 791 (2018).

[51]P. Rodríguez-Sevilla , Y. Zhang , P. Haro-González , F. Sanz-Rodríguez , F. Jaque, J. G. Solé, X. Liu , and D. Jaque, Adv. Mater. 28, 2421 (2016).

[52]L. Aigouy, G. Tessier, M. Mortier, B. Charlot, Appl. Phys. Lett. 87, 184105 (2005).

[53]C. D. S. Brites, P. P. Lima, N. J. O. Silva, A. Millan, V. S. Amaral, F. Palacio and L. D. Carlos, New J. Chem. 35, 1177 (2011).

[54]F. Vetrone, R. Naccache, A. Zamarron, A. Juarranz de la Fuente, F. Sanz-Rodriguez, L. Martinez Maestro, E. Martin Rodriguez, D. Jaque, J. Garcia Solé and J. A. Capobianco, ACS Nano 4, 3254 (2010).

[55]A. Wickberg, J. B. Mueller, Y. J. Mange, J. Fischer, T. Nann and M. Wegener, Appl. Phys. Lett. 106, 133103 (2015).

[56]L. Aigouy, Y. De Wilde, M. Mortier, J. Giérak and E. Bourhis, Appl. Opt. 43, 3829 (2004).

[57]G. Baffou, P. Berto, E. Bermúdez Ureña, R. Quidant, S. Monneret, J. Polleux and H. Rigneault, ACS Nano 7, 6478 (2013).

[58]S. Gomès, A. Assy and P.-O. Chapuis, Phys. Stat. Sol. A 212, 477 (2015).